Mon. Not. R. Astron. Soc. **327,** 799–807 (2001)

On the X-ray time-lags in the black hole candidates

O. Kotov,[1,2] E. Churazov[2,1]★ and M. Gilfanov[2,1]
[1]*Space Research Institute (IKI), Profsoyuznaya 84/32, Moscow 117810, Russia*
[2]*Max-Planck-Institut für Astrophysik, Karl-Schwarzschild-Strasse 1, 85741 Garching, Germany*

Accepted 2001 June 14. Received 2001 June 14; in original form 2001 March 13

ABSTRACT

It is shown that the energy dependence of the time-lags in Cygnus X-1 excludes any significant contribution of the standard reflected component to the observed lags. The conclusion is valid in the 0.1–10 Hz frequency range where time-lags have been detected with sufficient significance. In fact, the data hint that the reflected component is working in the opposite direction, reducing the lags at energies where the contribution of the reflected component is significant.

We argue that the observed logarithmic dependence of time-lags on energy could be due to the small variations of the spectral index in the frame of a very simple phenomenological model. We assume that an optically thin flow/corona, emitting a power law like spectrum, is present at a range of distances from the compact object. The slope of the locally emitted spectrum is a function of distance, with the hardest spectrum emitted in the innermost region. If perturbations with different time-scales are introduced to the accretion flow at different radii, then X-ray lags naturally appear, caused by the inward propagation of perturbations on the diffusion time-scales.

Key words: accretion, accretion discs – stars: individual: Cygnus X-1 – X-rays: general – X-rays: stars.

1 INTRODUCTION

The strong variability of the X-ray flux is a generic property of the black hole binaries in the so-called hard state (see e.g. van der Klis 1994). While it is usually assumed that X-ray emission is produced via Comptonization of the low-frequency photons by an optically thin cloud of hot electrons (e.g. Sunyaev & Truemper 1979), the nature of the strong variations is not so well understood. One of the possible clues to the origin of the variability may be connected with the presence of the time-lags between the light curves in different energy bands. The time-lags were first discovered in the early observations of Cygnus X-1 (Priedhorsky et al. 1979; Nolan et al. 1981) and confirmed in the numerous subsequent observations of Cygnus X-1 and other black hole candidates. In the vast majority of cases, hard photons lag relative to the soft ones. From observations it was found that (i) the value of the time-lag depends on frequency, (ii) the time-lag depends on the energy separation between two bands approximately logarithmically (e.g. Miyamoto & Kitamoto 1989), (iii) the cross-correlation function between any two energy bands peaks at zero lag (Maccarone, Coppi & Poutanen 2000 and references therein). A comprehensive description of the observed Cygnus X-1 variability and time-lags are given by Nowak et al. (1999a,b) and Pottschmidt et al. (2000). Recent reviews of the observed lags and theoretical models are given by Poutanen (2001a,b).

We discuss the time-lags below, using *RXTE* data on Cygnus X-1 as an example. In Section 2 we show that the observed energy dependence of the time-lags excludes a significant contribution of the standard reflected component to the time-lags in Cygnus X-1. In Section 3 we introduce a simple phenomenological model of the time-lags which naturally explains the logarithmic energy dependence of the time-lags. In Section 4 we discuss the possibility of explaining the lags as being caused by diffusive propagation of the perturbations in the accretion flow. In Section 5 we discuss the implications of the results. Section 6 summarizes our finding.

2 TIME-LAGS CAUSED BY THE LIGHT CROSSING-TIME OF THE REFLECTOR

For the hard X-ray state of Cygnus X-1, one of the popular models assumes that an optically thick and geometrically thin disc is truncated at some radius from the compact object and that most of the observed X-ray emission comes from the more compact optically thin region located closer to the black hole (e.g. Esin, McClintock & Narayan 1997; Zdziarski, Lubinski & Smith 1999). A fraction of the hard X-ray photons emitted by the central region can be intercepted by the optically thick disc and re-emitted again.

★E-mail: churazov@mpa-garching.mpg.de

This re-emitted/reprocessed component, also called the 'reflected' component, has a very distinct spectral shape (e.g. Basko, Sunyaev & Titarchuk 1974; George & Fabian 1991). If matter in the optically thick disc is neutral or weakly ionized then the spectrum of the reflected component is harder (in the standard X-ray band) than the illuminating spectrum and it also contains a prominent iron fluorescent Kα line. Because of the delay of the photons which travelled from the emission region to the reflector and then to the observer, hard lags may appear naturally (e.g. Poutanen 2001b).

In the presence of the direct and reflected components the observed spectrum $S(E, t)$ at time t can be written as:

$$S(E,t) = D(E,t) + R(E,t), \tag{1}$$

where $D(E, t)$ and $R(E, t)$ are the time-dependent spectra of the direct and reflected components respectively. Assuming that the direct component varies in intensity only and not in shape, then we can write

$$D(E,t) = A(t)D(E), \tag{2}$$

and neglecting the dependence of the reflected component spectral shape on the incident and emission angles, the reflected component can be written as:

$$R(E,t) = \frac{\Omega}{2\pi} R(E) \int T(\tau)A(t-\tau)\,\mathrm{d}\tau, \tag{3}$$

where $R(E)$ is the energy spectrum of the reflected component calculated for the reflector subtending the solid angle of 2π, $A(t)$ is the normalization of the direct component and $T(t)$ is the reflected component transfer function, which characterizes the time-dependence of the intensity of the reflected component in response to an infinitely short flare of the direct component. In the above expression, $T(t)$ is normalized such that $\int_0^\infty T(t)\,\mathrm{d}t = 1$ and the contribution of the reflected component to the time-averaged spectrum is expressed through the standard factor $\Omega/2\pi$, where Ω is the total solid angle subtended by the reflector. The expression (1) can be rewritten as

$$S(E,t) = A(t)D(E) + \frac{\Omega}{2\pi} R(E) \int T(\tau)A(t-\tau)\,\mathrm{d}\tau. \tag{4}$$

Further, assuming that contribution of the reflected component to the total spectrum is small, one can write the expression for a frequency-resolved spectrum, introduced in Revnivtsev, Gilfanov & Churazov (1999):

$$S(E,f) = |\hat{S}(E,f)| \approx |\hat{A}(f)|D(E)\sqrt{1 + 2\frac{\Omega}{2\pi}\frac{R(E)}{D(E)}\mathrm{Re}[\hat{T}(f)]}$$

$$\approx |\hat{A}(f)|\left\{D(E) + \frac{\Omega}{2\pi}R(E)\mathrm{Re}[\hat{T}(f)]\right\}. \tag{5}$$

The normalization factor $\Omega/2\pi$ has the same meaning as for the energy spectrum. In some simple cases, e.g. for an isotropic source of primary radiation, Ω is the solid angle subtended by the reflector. In the case of an anisotropic source, the factor $\Omega/2\pi$ also accounts for the difference in the radiation flux towards the reflector and towards the observer. The equivalent width of the iron line in the frequency-resolved spectrum is then obviously

$$EW(f) \approx EW_\mathrm{t}\mathrm{Re}[\hat{T}(f)], \tag{6}$$

where EW_t is the equivalent width in the total source spectrum. From the above expression, it follows that the equivalent width of the iron line in the frequency-resolved spectrum should be smaller than the equivalent width in the total source spectrum. For instance, for a reflector with a characteristic light crossing-time τ, the equivalent width should be very small at frequencies much higher than $1/\tau$, where $\mathrm{Re}[\hat{T}(f)] \ll 1$. Using similar arguments, Revnivtsev et al. (1999) and Gilfanov, Churazov & Revnivtsev (2000) set an upper limit on the effective size of the reflector in Cygnus X-1 of $\sim 50\,R_\mathrm{g}$. Here R_g is the gravitational radius for a 10-$\mathrm{M}_\odot$ black hole. We note here that expression (6) was derived assuming a linear relation between variations in the direct and reflected components (see equation 3). If on the contrary the variations of the direct $D(E, t)$ and reflected $R(E, t)$ components are completely uncorrelated, then

$$S(E,f) = |\hat{S}(E,f)| = \sqrt{|\hat{D}(E,f)|^2 + |\hat{R}(E,f)|^2}$$

$$\approx |\hat{D}(E,f)|\left[1 + \tfrac{1}{2}|\hat{R}(E,f)|^2/|\hat{D}(E,f)|^2\right]. \tag{7}$$

In this case, the equivalent width of the reflected component in the frequency-resolved spectrum depends on the power density spectra of both direct and reflected components, and scales as the square of the factor $(\Omega/2\pi)$ determined from total source spectrum fitting.

One can further test the hypothesis of the large effective size of the reflector using the time-lags. Assuming again that the light curve in any energy band can be expressed through equation (4), the expected phase-lag $\phi(E, f)$ between the given energy E and much lower energy (where the contribution of the reflected component is negligible and the spectrum is solely due to the direct component) can be written as

$$\tan(\phi(E,f)) = \frac{\mathrm{Im}[\hat{S}^*(E,f)\hat{D}(E,f)]}{\mathrm{Re}[\hat{S}^*(E,f)\hat{D}(E,f)]}$$

$$\approx \frac{(\Omega/2\pi)R(E)\mathrm{Im}[\hat{T}]}{D(E) + (\Omega/2\pi)R(E)\mathrm{Re}[\hat{T}]}$$

$$\approx \frac{\Omega}{2\pi}\frac{R(E)}{D(E)}\mathrm{Im}[\hat{T}(f)]. \tag{8}$$

Therefore in this approximation, the frequency-dependence of the phase-time-lags is a result of an imaginary part of the Fourier transform of the transfer function. The energy-dependence of the lags is simply the ratio of the reflected and direct spectral components. Because $D(E)$ is assumed to be a smooth function of energy, the time-phase-lag as the function of energy should contain a prominent iron line with an equivalent width comparable to the equivalent width of the line in the reflected component, i.e. a much larger equivalent width than in the total spectrum.

In order to assess the possible contribution of the reflected component in the observed time-lags in Cygnus X-1, we calculated lags in the narrow energy channels. For our analysis we used publicly available data of *Rossi X-ray Timing Explorer* observations P10238 performed between 1996 March 26 and 31, with a total exposure time of $\sim$70 ks (we used observations with all 5 Proportional Counter Units turned on). We used PCA data in the 'Generic Binned' mode, having (1/64) s $\sim$16 ms time-resolution in 64 energy channels, covering the whole PCA energy band. The lags were calculated for every channel above 3.7 keV, with respect to the count rate in the 2.8–3.7 keV energy band. The resulting energy dependence of the time-lag at frequencies of the order of 2.5 Hz is shown in Fig. 1.[1] For comparison, in the same figure we plot an

[1] Time-lags at other frequencies in the range from $\sim$0.6 to $\sim$10 Hz have approximately similar energy dependence (see Fig. 2).

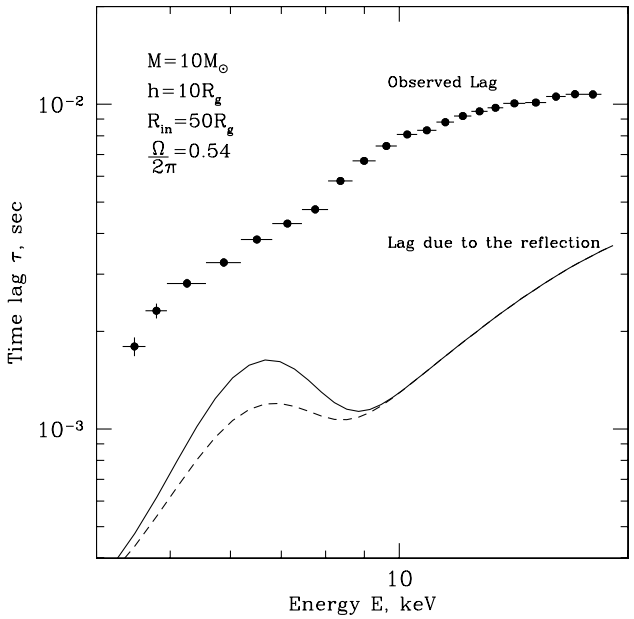

Figure 1. The energy dependence of the time-lag in Cygnus X-1 in the hard state at the frequency of 2.5 Hz. For comparison, the energy dependence of the time-lags expected in the model with extended reflector is shown. For the upper curve we used the relative normalization of the Gaussian and the reflected continuum obtained from the fit to the total Cygnus X-1 spectrum during observation 10238-01-08-00 (Gilfanov et al. 1999). For the lower curve the normalization of the Gaussian was chosen such that the equivalent width of the line with respect to the reflected continuum is ∼1 keV. The latter value is characteristic for an angle-averaged reflection from a neutral matter with a normal abundance of heavy elements.

expected energy dependence of the lags caused by the reflected component, according to equation (8). Normalization of the expected curve is arbitrary. Here we used the averaged spectrum of the source during this observation as $D(E)$. The reflected component $R(E)$ was calculated using XSPEC V11 (Arnaud 1996) model PEXRAV of Magdziarz & Zdziarski (1995), plus a Gaussian using an energy of 6.4 keV. The resulting spectrum has been convolved with the PCA energy response matrix. Note that the expected lags were calculated using equation (8), i.e. with respect to the energy range where the contribution of the reflected component was assumed to be zero. Therefore, the expected lags do not go to zero at energies < 4 keV. The two curves shown in Fig. 1 differ in the normalization of the Gaussian added to the reflected continuum. For the upper curve we used relative normalization of the Gaussian and reflected continuum obtained from the fit to the total Cygnus X-1 spectrum during observation 10238-01-08-00 (Gilfanov, Churazov & Revnivtsev 1999). For the lower curve the normalization of the Gaussian was chosen such that the equivalent width of the line with respect to the reflected continuum is ∼1 keV. The latter value is characteristic for an angle-averaged reflection from a neutral matter with a normal abundance of heavy elements.

One can see from Fig. 1 that the lags caused by the reflected component should contain a prominent feature at the energy ∼6.4 keV. We stress again that this feature should be much more prominent in the lags than in the averaged spectrum, where the iron line provides at most 10 per cent of the relative deviation of the observed spectrum from a power-law fit. Clearly no such feature is present in the observed lags. We therefore conclude that the observed lags are predominantly not caused by the reflected component.

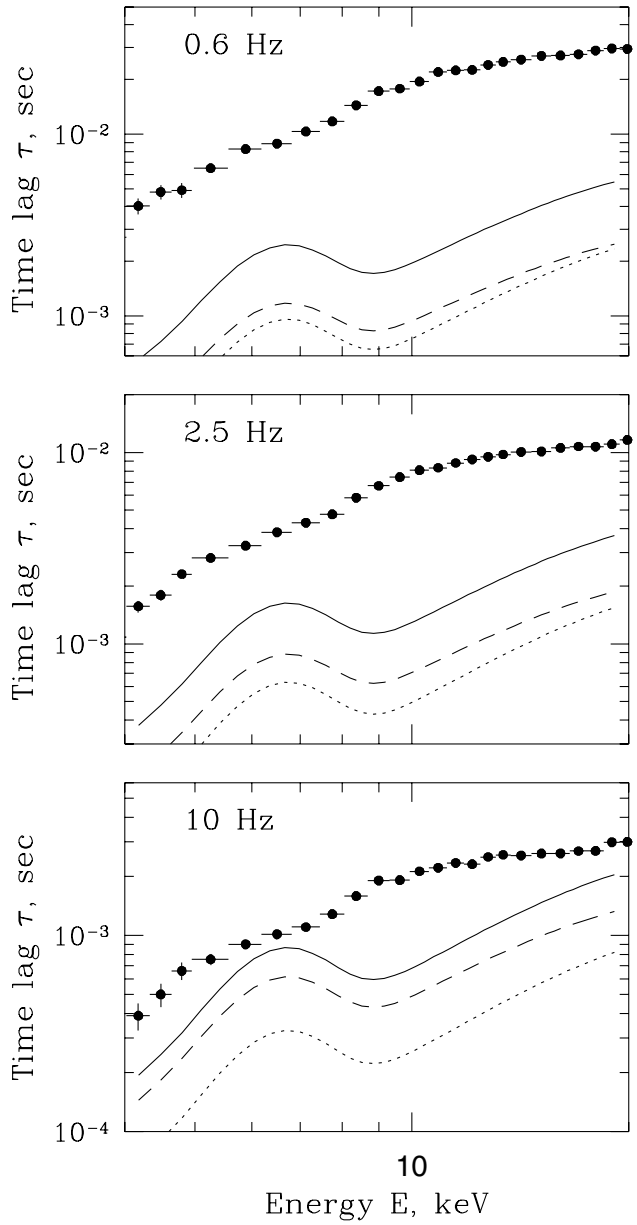

Figure 2. The energy dependence of the time-lag in Cygnus X-1 in the hard state at different frequencies. For comparison, we show the expected curves for the models where reflected component originates from a flat disc with a central hole illuminated by the compact source located at the height $h = 10R_g$ above the disc surface. The different curves correspond to the following sets of model parameters: $R_{in} = 50R_g$; $\Omega/2\pi = 0.54$ (solid line), $R_{in} = 10R_g$; $\Omega/2\pi = 0.7$ (dashed line), $R_{in} = 50R_g$; $\Omega/2\pi = 0.2$ (dotted line) respectively.

One can use the same argument in order to constrain the geometry of the reflecting region. Indeed, the lack of the iron line feature in the observed energy dependence of the time-lags imply certain constraints on the combination of the reflected component strength and the duration of the time delay caused by the finite size of the reflector. In Fig. 2 we show the observed energy dependence of the time-lags at three represented frequencies: 0.6, 2.5 and 10 Hz. For comparison, in the same plot we show the expected time-lags for different geometries of the reflector and different strengths of the reflected component. Three basic models have been considered.

(A) A point isotropic source above the flat disc with the hole in the middle. The height h of the source above the disc plane is set to $10R_g$, the size of the hole R_{in} in the disc is set to $50R_g$. Here R_g is the gravitational radius for a $10\,M_\odot$ black hole. The factor $\Omega/2\pi$, calculated for this geometry, is $\simeq 0.2$.

(B) The same geometry as for A, but the strength of the reflected component was enhanced, so that effective parameter $\Omega/2\pi$ is 0.54. This is possible if, for example, the source of the primary emission is anisotropic and more emission is coming towards the disc than towards the observer. The particular value of the normalization of the reflected component in this model was taken from the fit to the total Cygnus X-1 spectrum during observation 10238-01-08-00 (Gilfanov et al. 1999).

(C) The same geometry as for A, but for $R_{in} = 10R_g$. The factor $\Omega/2\pi$, calculated for this geometry, is $\simeq 0.7$.

The transfer functions in the form $(\Omega/2\pi)T(t)$ for models A and C are shown in Fig. 3 for two values of the disc inclination θ (0° and 50°). Model B obviously has the same shape of the transfer function as model A and is different only in normalization. For comparison we also show the transfer function for a concave disc with the dependence of disc height over radius adopted from Shakura & Sunyaev (1973). For the frequency range considered here such concave discs do not differ from the flat discs.

The lags expected in these models (for inclination $\theta = 50°$) are shown in Fig. 2. The model curves were calculated for the equivalent width of the Fe Kα line with respect to the reflected continuum obtained from the fit of the time-averaged source spectrum. As was mentioned above, the lack of a prominent iron feature in the energy dependence of the time-lags suggests that the lags are largely not a result of the reflection. Moreover, the lags expected in models B and C at 10 Hz must produce a clear feature at 6.4 keV in contradiction to the data. Even for model A, expected lags can be only marginally 'hidden' in the observed lags. There are, however, many uncertainties and simplifications in the models discussed above. In particular, we have neglected the dependence of the reflected component spectrum on the incident angle. Also the surface of the reflector (upper few Thomson optical depths) may not be smooth and flat, but wrinkled. Furthermore, ionization of the reflector surface will modify the spectrum of the reflected component. Finally, all relativistic effects associated with reflection from the inner regions of the accretion disc (see e.g. Campana & Stella 1995) have been ignored. Accounting for all these effects may modify the normalization and shape of the energy dependence of the time-lags by a factor of a few.

Perhaps the most dubious assumption is the 'linear' response of the reflected component to the variations of the illuminating flux. Recent analysis (e.g. Nayakshin & Kallman 2000) shows that the shape of the reflected component can vary in a complicated fashion in response to an increase of the primary flux. Therefore, the conservative conclusions of this section are that (i) the 'linear' reflected component, containing prominent fluorescent line at 6.4 keV, is not responsible for the observed lags and (ii) some of the source/reflector geometrical models can be definitely excluded.

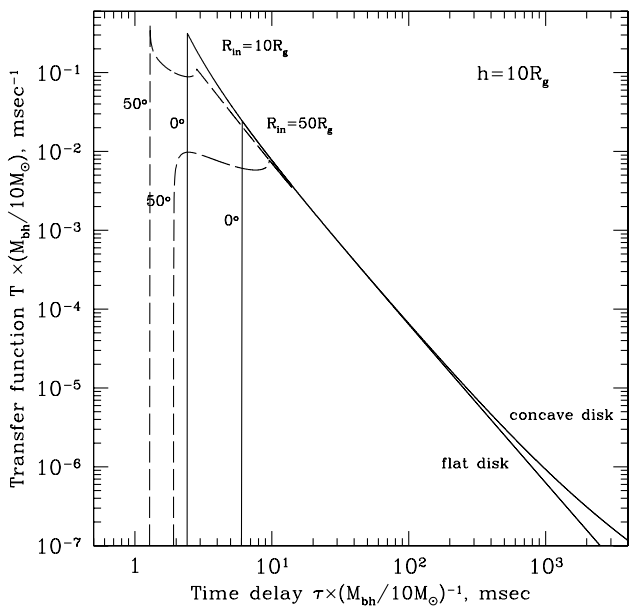

Figure 3. The transfer functions $(\Omega/2\pi)T(t)$ for an isotropic point source of primary radiation located at $h = 10R_g$ above a flat or concave disc with an inner radius of $R_{in} = 10$ and $50\,R_g$ and an inclination of 0° and 50°.

3 TIME-LAGS CAUSED BY VARIATIONS OF THE POWER-LAW INDEX

The spectrum of Cygnus X-1 in the 2–20 keV energy band can be reasonably well approximated by a power law. Deviations, in particular those caused by the reflected component, are present, but their amplitude relative to the power-law component is usually less than 10 per cent in this energy range. We assume below that at any moment of time the spectrum can be represented as a power law:

$$S(E,t) = A(t)E^{-\alpha(t)}, \tag{9}$$

where $A(t)$ is the normalization of the power law as a function of time and $\alpha(t)$ is the photon index, which is also a function of time. For simplicity, we set $\alpha(t) = \alpha_0 - \beta(t)$, where α_0 is a photon index of the time-averaged spectrum and $\beta(t)$ is the time-variable part of the photon index. Assuming that $\beta(t) \ll \alpha_0$, the spectrum of the source can be rewritten as

$$S(E,t) = A(t)E^{-\alpha_0}[1 + \beta(t)\ln E]. \tag{10}$$

The phase-lag ϕ at a given frequency f can then be written through the Fourier transforms $\hat{S}^*(E,f)$ of the source light curves at two different energies E_1 and E_2 as:

$$\begin{aligned}\sin\phi &= \frac{\mathrm{Im}[\hat{S}^*(E_1,f)\hat{S}(E_2,f)]}{|S(E_1,f)||S(E_2,f)|}\\ &\approx \frac{\mathrm{Im}\{[\hat{A}^* + (\widehat{\beta A})^*\ln E_1][\hat{A} + (\widehat{\beta A})\ln E_2]\}}{\hat{A}^*\hat{A}}\\ &\approx \frac{\mathrm{Im}[\hat{A}^*(\widehat{\beta A})]}{\hat{A}^*\hat{A}}\ln\frac{E_2}{E_1}.\end{aligned} \tag{11}$$

In the above expression we neglected the terms of the order of $O(\beta^2)$. Thus the assumption that the spectrum has a power-law shape at any moment of time and the variations of slope are small automatically implies that phase-lags (and consequently time-lags) scale as $\ln(E_2/E_1)$.

3.1 Universal slope flux correlation?

It is clear that if variations of the slope $\beta(t)$ and the normalization $A(t)$ are random and incoherent then the time-lag is zero. If these two quantities are correlated then a non-zero lag may appear. The simplest assumption would be a linear correlation between the

slope and normalization (i.e. between the slope and flux):

$$\beta(t) = \gamma[A(t) - A_0], \tag{12}$$

where A_0 is the normalization of the time-averaged spectrum and γ is the coefficient of linear proportionality between the variations of normalization and slope. We note here that the correlation between the slope of the spectrum and the energy release naturally appears in many models involving Comptonization of the soft photons in the cloud of hotter electrons.

The expression for phase-lags is then further reduced to

$$\sin\phi = \frac{\mathrm{Im}[\hat{A}^*(\widehat{A^2})]}{\hat{A}^*\hat{A}}\gamma \ln\frac{E_2}{E_1}. \tag{13}$$

In this approximation, the sign and the amplitude of the lags would simply reflect the properties of the flux variations on different time-scales. Unfortunately the function (13), calculated for the observed light curves, changes the sign several times within the frequency range where hard lags are observed. This means that the simple linear correlation between the flux and the slope of the spectrum can be excluded, or that the sign of the correlations between flux and slope also has to change sign in order to keep the sign of (13) the same at all frequencies. We note here that change of the slope/flux correlations sign at different time-scales was indeed reported for Cygnus X-1 (Li, Feng & Chen 1999). Thus it is clear that the simple linear correlation between the slope and the flux fails to produce observed hard lags and more complicated models have to be invoked.

4 TIME-LAGS CAUSED BY ACCRETION

In this section we construct a simple model which attributes the lags to the propagation of perturbations in the accretion flow from the outer to inner regions. As was discussed by Lyubarskii (1997) and Churazov, Gilfanov & Revnivtsev (2001), the strong variability of the X-ray flux over a very broad dynamic range of time-scales suggests that different time-scales are introduced to the accretion flow at different distances from the compact source. One might think, in terms of the effect on the mass accretion rate of the magneto-hydrodynamic turbulence, which serves as a source of the viscosity in the accretion flow through the fluctuating magnetic stresses (e.g. Balbus & Hawley 1991; Hawley, Gammie & Balbus 1995; Brandenburg et al. 1995). The perturbations introduced at large distances from the compact object are then propagated down to the region of main energy release and cause observed variations in the X-ray flux. If the propagation of the perturbations in the radial direction is a result of viscous diffusion, then the very fact that we observe strong variations of the X-ray flux means that the propagation/diffusion time from a given radius r_0 is comparable to or shorter than the time-scale of perturbations introduced to the flow at this radius r_0. Otherwise these perturbations would be completely washed out before reaching the innermost region. This in turn means that lags could naturally appear in such a situation if the locally emitted spectrum is a function of radius r. Of course, the energy budget of the accretion flow far from the innermost region is small, but the observed lags are also small, of the order of 0.1 rad. We then tested the feasibility of this model using the following assumptions.

(i) Statistically independent (incoherent) perturbations are introduced to the accretion flow at different distances from the compact source. The characteristic time-scale of these perturbations is a function of radius.

(ii) We further assume that the shape of the locally emitted spectra depends on radius and it is getting progressively softer as the distance from the compact object increases.

The light curve at a given energy E is:

$$L(E,t) = \int\int\int D(r_0,t_0)G(r,r_0,t-t_0)\epsilon(r)S(E,r)\,\mathrm{d}r\,\mathrm{d}r_0\,\mathrm{d}t_0, \tag{14}$$

where $D(r_0, t_0)$ is an initial perturbation introduced to the flow at radius r_0 and time t_0, $G(r, r_0, t - t_0)$ is the Green function, which describes propagation of the perturbations from radius r_0 to r, $S(E, r)$ is the shape of the locally emitted spectrum at the radius r and $\epsilon(r)$ is the total luminosity of the accretion flow emitted at a given radius. The assumption of the statistical independence of perturbations introduced at different radii implies that quantities like power density or cross spectra can be calculated independently for each initial radius and then averaged over range of initial radii. The Fourier transform $\hat{L}(E, f)$ of the X-ray light curve is then

$$\hat{L}(E,f) = \int \hat{D}(r_0,f)\int \hat{G}(r,r_0,f)\epsilon(r)S(E,r)\,\mathrm{d}r\,\mathrm{d}r_0, \tag{15}$$

where $\hat{D}(r_0, f)$ is the Fourier transform of the perturbations introduced to the flow at the radius r_0, $\hat{G}(r, r_0, f)$ is the Fourier transform of the Green function, f is the frequency. From the above equation it is clear that in this approximation the time-lags are solely caused by the properties of the Green function and the dependence of the spectral shape on radius. For our toy model we choose the simplest possible version with $\epsilon(r) \propto 1/r^2$ per unit dr. In order to calculate the phase- and time-lags we created two artificial light curves in the 'soft' and 'hard' bands, assuming simple laws of emissivity in these bands:

$$S(r) = \epsilon(r)S(E_{\mathrm{soft}}, r) = \frac{1}{r^2}$$

$$H(r) = \epsilon(r)S(E_{\mathrm{hard}}, r) = \frac{1}{r^2}h(r), \tag{16}$$

where $h(r)$ is a decreasing function of the radius. For simplicity we assume that propagation of the perturbations can be characterized by the Green function of Lynden-Bell & Pringle (1974), describing diffusion in the geometrically thin disc approximation (see also Lyubarskii 1997), i.e.

$$G(r,r_0,t) \propto \frac{r^{-1/4}}{t}\exp\left[-\frac{r_0^{1/2l}+r^{1/2l}}{4t}\right]I_l\left[\frac{r^{1/4l}r_0^{1/4l}}{2t}\right], \tag{17}$$

where $I_\nu[x]$ is the Bessel function of imaginary argument. For the parameter l we use the value of 1/3 appropriate for a standard α disc with constant ratio H/r, where H is a half-thickness of the disc. In this equation and below we measure radius r in units of r_{min}, which is supposed to be the characteristic radius of the inner region of the accretion flow where most of the energy is released. Time is measured in units of the characteristic diffusion time $k^2 \times r_{\mathrm{min}}^{1/2l}$, where k is the effective diffusion coefficient.

Two simple versions of the function $h(r)$ (hereafter the 'hardness' function) are shown in Fig. 4. The dotted line shows the case when the slope of the locally emitted spectrum is the same at all distances from the compact object, but it abruptly hardens within the innermost region. The solid line shows the case when the locally emitted spectrum gradually hardens as the distance from the compact object decreases. In Fig. 5, light curves in the soft and hard energy bands are shown, assuming the $h(r)$ function with the abrupt jump. Here the initial radius r_0 was set to 30 and the initial

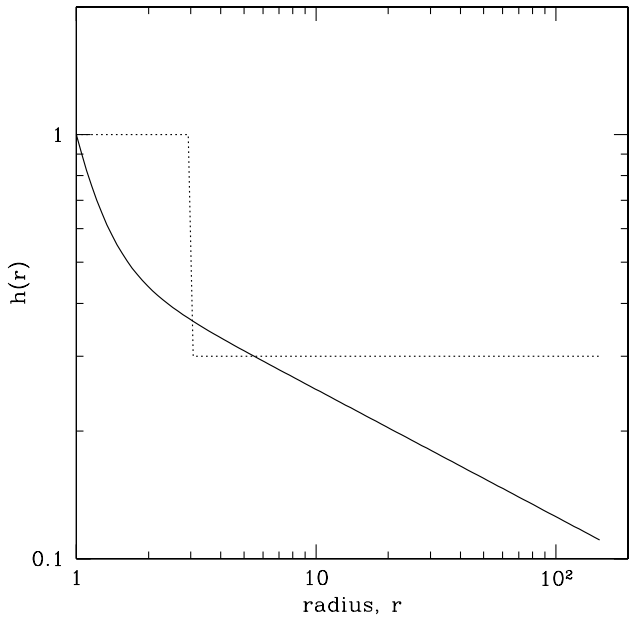

Figure 4. Two versions of the $h(r)$ function, used in the simulations. The dotted line shows the $h(r)$ function when the locally emitted spectrum has the same slope at all distances from the compact object except for the innermost region, where the spectrum is harder. The solid line shows the case where the spectrum gradually steepens with distance from the compact object. The amplitude of the $h(r)$ function variations affects the absolute value of the time-/phase-lag.

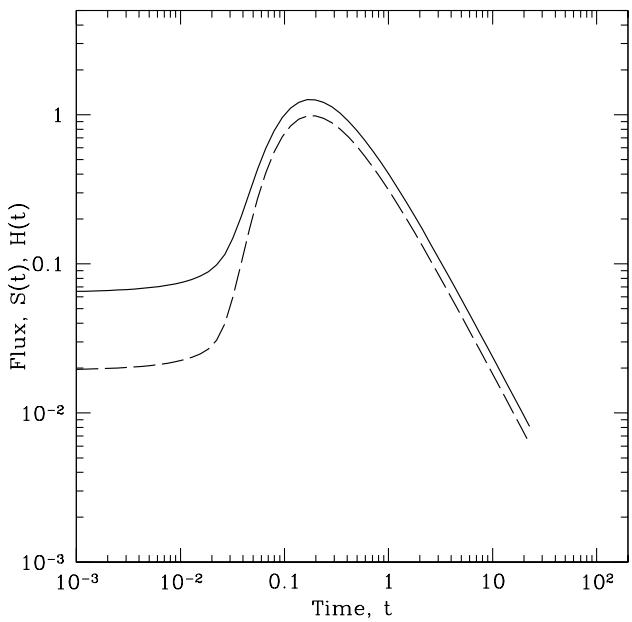

Figure 5. Light curves in two energy bands (soft – solid line, hard – dashed line) for the $\delta(t)$ perturbation at the initial radius $r_0 = 30$.

perturbation was assumed to be a δ-function in time and radius. Initially, the locally emitted spectrum is soft and it hardens when perturbation spreads all the way down to the minimal radius. After that moment, the hardness of the spectrum remains practically unchanged.

We then calculated the phase-lags fixing the initial radius at $r_0 = 30$ and varying the characteristic frequency of the initial perturbation. The dependence of the phase-lag on frequency is shown in a Fig. 6. The solid line in this figure shows the phase-lag

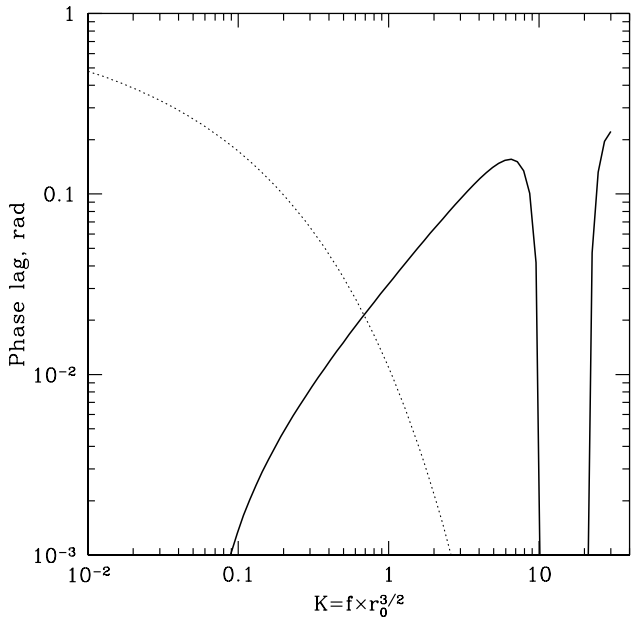

Figure 6. The phase-lag (solid line) as a function of frequency for the perturbations introduced at fixed initial radius $r_0 = 30$. The dotted line show the value of the transfer function power $|\int \hat{G}(r, r_0, f)\epsilon(r)\,\mathrm{d}r|^2$, which characterizes the suppression of the power of the initial perturbation at a given frequency caused by diffusive spreading.

(in radians) as a function of frequency expressed in units of inverse characteristic diffusion time for a given initial radius $r_0^{3/2}$. These lags were calculated for the $h(r)$ function with a jump (see Fig. 4), but for the smoother $h(r)$ the resulting lags are practically the same. The dotted line in the same figure shows the value of the transfer function power $|\int \hat{G}(r, r_0, f)\epsilon(r)\,\mathrm{d}r|^2$. It characterizes to what extent an amplitude of a perturbation at a given frequency f is suppressed in the observed light curve caused by diffusive spreading. Values of the order of 10^{-2} imply that 'local' perturbations at r_0 with an amplitude of the order of unity would result in $\sim$10 per cent variations in the innermost region where bulk of energy is released.

In order to calculate phase-lags associated with the perturbations generated at different radii we made further the simplifying assumption that at every initial radius r_0, instabilities generate a single frequency which scales as a characteristic diffusion time at this radius,[2] i.e. $f(r_0) = Kr_0^{-3/2}$, where K is a parameter. From Fig. 6 one would expect the lags to increase with the increase of K, unless K is too large. The resulting phase-lags for two versions of the 'hardness' function are shown in Fig. 7. The resulting phase-lags grow weakly with frequency and reach $\sim$0.1 rad before falling sharply. The amplitude of the phase-lags and the dependence of the lags on frequency are thus regulated by two major parameters: (i) the amplitude of the spectral variations as a function of radius and (ii) the relation between the time-scale of perturbations (locally generated at radius r_0) and the diffusion time-scales from r_0 down to much smaller radii. We stress that under the assumption of the perturbation frequencies being different at different radii, the phase-lags do not depend on the shape of the power density spectra and are solely determined by the Green function and the 'hardness' function.

[2] Note that for the α disc, with a constant ratio of the disc height to the radius, the characteristic diffusion time and Keplerian time scale similarly.

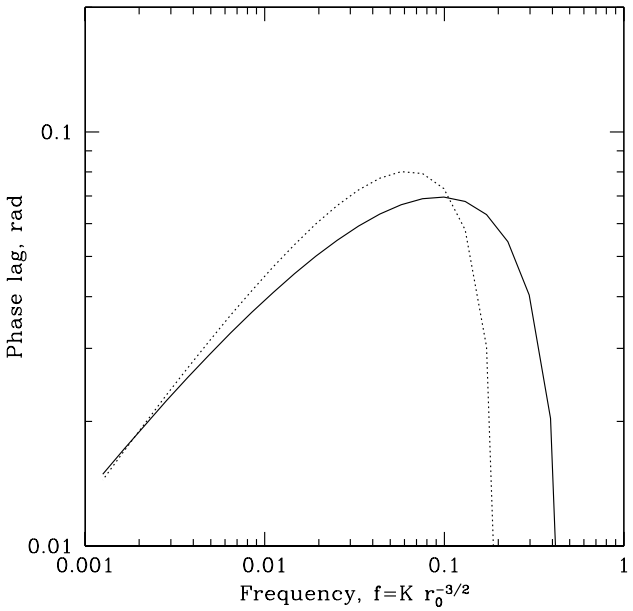

Figure 7. The phase-lags for two versions of $h(r)$. Frequency introduced at radius r_0 is assumed to scale as $Kr_0^{-3/2}$ with $K = 1$.

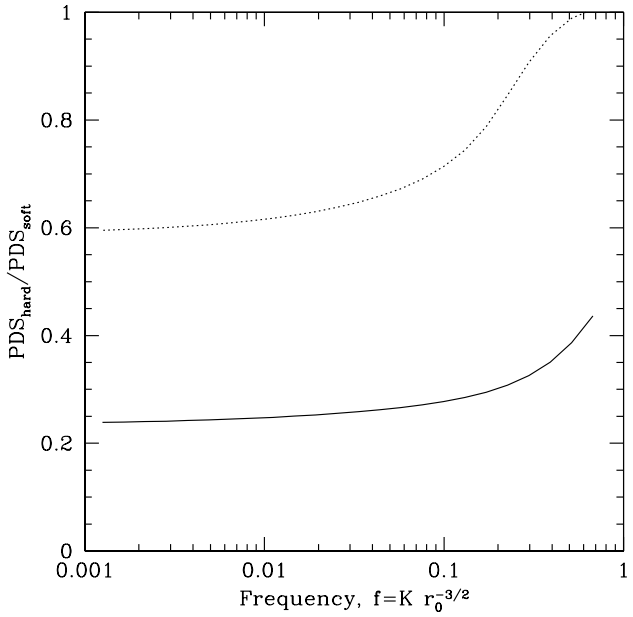

Figure 8. The ratio of the power density spectra of the hard and soft light curves (see equation 16) for two versions of $h(r)$.

In the model considered above, one would expect that the power density spectra in different energy bands should have a somewhat different shape, as a result of the influence of the 'hardness' function. In Fig. 8 we show the ratio of the power density spectra in the 'hard' and 'soft' bands as a function of frequency. This ratio is again independent of the shape of the power density spectrum and is governed by the Green function and the 'hardness' function. One can see that, as expected, the ratio of the power density spectra increases with frequency.

For completeness we also calculated time-lags using the same choice of the 'hardness' function, but instead of a diffusion Green function we substitute a Green function appropriate for free-fall from a given radius r_0. This is equivalent to the assumption that

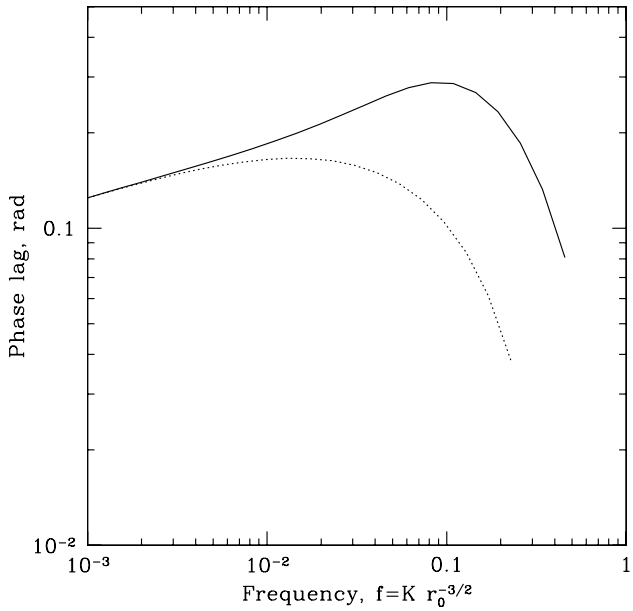

Figure 9. The lags for the free-fall model for $K = 1$ and $K = 0.5$.

distinct blobs of emitting matter are falling towards the compact source with the velocity $v \propto r^{-1/2}$. The resulting lags are shown in Fig. 9. As, in this case, no viscous spreading is present, the absolute value of the lags is higher for the same choice of the 'hardness' function and the parameter K.

Finally, we stress that if the locally emitted spectrum at any radii is a power law then the observed lags will show logarithmic dependence on energy even if the total observed spectrum (integrated over all radii) is not well represented by a power law as assumed in the previous section. This follows from our assumption that perturbations generated at different radii are statistically independent.

4.1 'Anti-lags' caused by the reflected component

As we saw in Section 2, the observed energy dependence of the time-lags contradicts the assumption that hard lags are predominantly produced by the time delay of the reflected component with respect to the primary continuum. In particular (see Fig. 10), instead of a prominent hump at the energy of the iron fluorescent line, the observed lags seem to be slightly suppressed here. This behaviour might hint that reflected component somehow works in the opposite direction and reduces the lags. We now discuss how such suppression could be introduced within the frame of the model considered above.

An assumption that a locally emitted spectrum has a power-law shape, with an index slowly varying with the distance from the compact object (so that hardest spectra are near the centre), will naturally lead to hard lags with a logarithmic dependence on energy. Let us now assume that the locally emitted spectra also contain a reflected component. Assuming that the overall geometry of the accretion flow resembles a truncated optically thick disc followed by an optically thin flow, one would expect the reflection fraction to be higher for spectra emitted at larger distances from the compact object, i.e. softer spectra (emitted at a larger distance from the compact object) have larger reflection fractions than harder spectra. In our model this means that reflected component is leading the harder spectrum. In this situation one would expect a

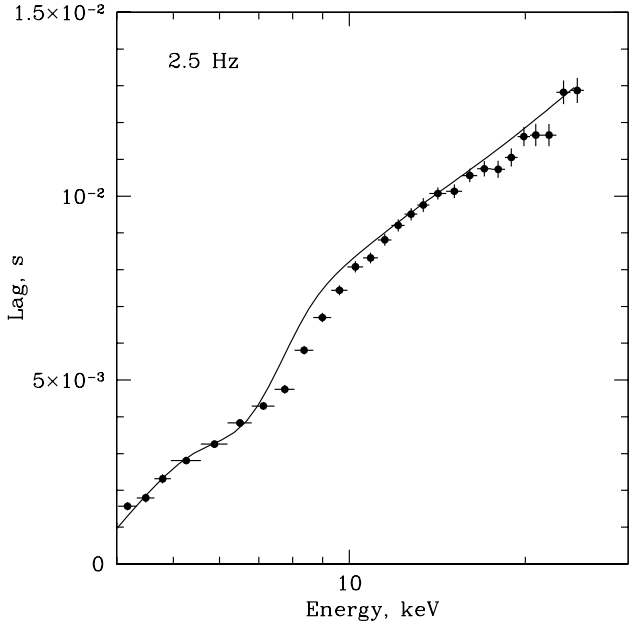

Figure 10. The time-lag at the frequency of 2.5 Hz as a function of $\log(E)$. See text for the description of the solid line.

slight modification of the logarithmic dependence of lags on energy caused by the reflected component. For simplicity we assumed that the lags are a result of two power-law spectra with the power law indices of 2.4 and 1.8 and the reflection fraction of $\sim$1 and $\sim$0.5 respectively. i.e. the light curve is

$$L(E,t) = S_1(E)\delta(t) + S_2(E)\delta(t-\Delta t), \quad (18)$$

where $\delta(t)$ is the Dirac δ-function. Reflected components in both spectra were smeared with a $\sim$0.8 keV Gaussian. In the limit of small frequencies one can easily write an expression for the time-lag as a function of energy for the light curve described by equation (18). The detailed shape of the energy dependence is affected by the strength of the reflection features in both spectra, the amount of smearing applied and the relative normalization of both spectra. One illustrative example, calculated for one particular choice of these parameters, is shown in Fig. 10 with a solid curve. This curve is not supposed to closely reproduce the data, but merely to demonstrate that the trend is in the right direction.

5 DISCUSSION

The properties of the hard lags observed in Cyg X-1 can be summarized as follows.

(i) In the hard state of Cygnus X-1, lags are observed very significantly in the frequency range of few 10^{-2} to a few 10 Hz. The phase-lag is a slightly growing function of frequency with a maximum phase lag of 0.1 rad between 3 and 10 keV (see recent data of Nowak et al. 1999a; Pottschmidt et al. 2000, also Fig. 11).

(ii) The energy dependence of the lags is approximately logarithmic (Miyamoto et al. 1988, Nowak et al. 1999a, see also Fig. 10) with the slight, but statistically significant, deviations from this dependence.

(iii) The cross-correlation function peaks at zero lag (Maccarone et al. 2000).

(iv) The coherence function is close to unity (Nowak et al. 1999a), at least in the middle of the frequency range, where lags are observed with high significance.

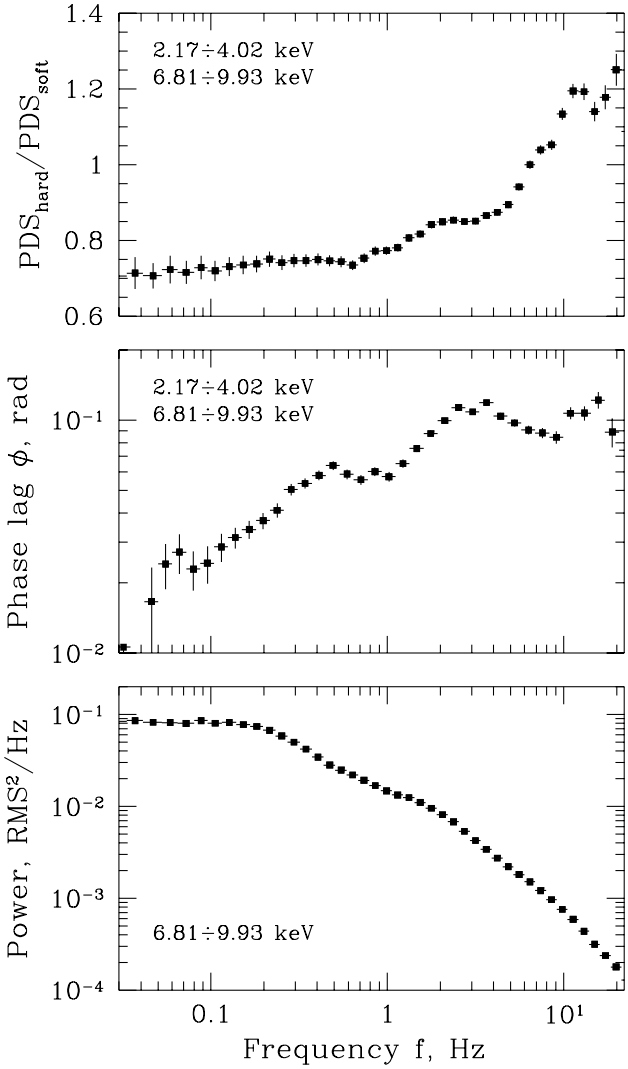

Figure 11. Cyg X-1: the observed power density spectrum (lower panel), the phase-lags (middle panel) and the ratio of the power density spectra in the two energy bands (upper panel).

Several different branches of models have been suggested as an explanation for the observed hard lags (see Poutanen 2001a,b for recent reviews). Our model belongs to the class of 'propagation' models as defined by Nowak et al. (1999b). Other models involving 'propagation' are those of Kato (1989), Nowak et al. (1999b), Böttcher & Liang (1999) and Misra (2000), (see also Manmoto et al. 1996). In fact, our version of the model is close to the original suggestions of Miyamoto et al. (1988) and Miyamoto & Kitamoto (1989) that 'a clump of matter … drifts from the outer (soft-X-ray-emitting) region to the inner (hard-X-ray emitting) region'.

The model is based on two major assumptions: (i) different time-scales are introduced to the accretion flow at different distances from the compact object, and the propagation time-scales are comparable to the time-scales of the perturbations, and (ii) the locally emitted spectra are power laws with smaller photon indices in the innermost region.

The logarithmic energy dependence of the lags follows directly from assumption (ii). The zero shift of the cross-correlation function and the coherence function close to unity naturally appear because most of the emission is coming from the innermost region and therefore most of the flux at all energies is released at the same

time (see Fig. 5). The dependence of the lags on frequency and maximal values of the lags are tuneable parameters of the model (through the dependence of the photon index on the radius – the 'hardness' function $h(r)$, and through the relation of the perturbation and propagation time-scales). The examples shown above (e.g. see Fig. 7) show that with reasonable assumptions one can approximately reproduce both the dependence of the lags on frequency and the maximal value of the phase-lag.

In addition, this model provides a natural explanation of the ratio of the power density spectra in different energy bands as a function of frequency (see Figs 8 and 11, upper panels) and offers a qualitative explanation for the deviations of the energy dependence of the lags from a simple logarithmic law (Fig. 10). Broadly, the model is consistent with the geometrical model in which the inside truncated optically thick disc is followed by the optically thin flow. At distances larger than the disc truncation radius, an optically thin flow also seems to be present and perhaps has a form of a corona sandwiching the disc (see arguments in Churazov et al. 2001). The latter assumption allows one to extend this model to the soft state of Cyg X-1 without any modifications.

Our assumption that each frequency in the observed flux variability is associated with some particular radius is of course a gross oversimplification. However, as a result of the suppression of the high-frequency variations in the course of diffusion, such a situation may take place in the accretion flow if the times scales of locally induced perturbations at a given radius are shorter than the radial diffusion time (Churazov et al. 2001). From Fig. 11 it is clear that there are several 'humps' in the power density spectrum of Cyg X-1. Assuming that this is an indication that perturbations arising at some particular radius of the accretion flow dominate at a range of frequencies, one would then expect the phase-lags to rise faster with frequency (compare Figs 7 and 6). It seems that such behaviour is indeed observed as the distinct regions of fast phase-lag rise (or time-lag shoulder – see Nowak et al. 1999a,b) in the Cyg X-1 data (Fig. 11).

The particular emission mechanism is not very important, as long as only the origin of the lags is considered. For example, emission could be caused by magnetic flares, as in the picture of Galeev, Rosner & Viana (1979) or Poutanen & Fabian (1999). In our model, flare spectra need not evolve (from soft to hard) themselves. They could be short and could occur at different distances from the compact object. The observed variability may not then be a result of individual flares but rather a result of a change of the number of active flares at a given moment of time. The model requires, however, that the spectra of more distant flares to be softer than those of the flares in the innermost region of the accretion flow.

6 CONCLUSIONS

We suggest a simple phenomenological model for the hard time-lags observed from the galactic black hole candidates, focusing on the approximately logarithmic energy dependence of the lags. The model attributes the lags to the viscous time-scales in the accretion flow and assumes that locally emitted spectra are power laws with photon indices smallest in the innermost region.

We also show that the energy dependence of the time-lags excludes the possibility that lags (in the 0.1–10 Hz range) are predominantly caused by the delay of the reflected component with respect to the illuminating continuum. This conclusion is derived under the assumption of a 'standard' neutral reflected component which linearly responds to the variations of the illuminating flux.

ACKNOWLEDGMENTS

This research has made use of data obtained through the High Energy Astrophysics Science Archive Research Center Online Service, provided by the NASA/Goddard Space Flight Center. OK acknowledges partial support by RFBR grants 00-15-96649 and 00-02-17124.

REFERENCES

Arnaud K. A., 1996, in Jacoby G., Barnes J., eds, Proc. ASP. Conf. Ser. Vol. 101, Astronomical Data Analysis Software and Systems V. Astron. Soc. Pac., San Francisco, p. 17
Balbus S. A., Hawley J. F., 1991, ApJ, 376, 214
Basko M. M., Sunyaev R. A., Titarchuk L. G., 1974, A&A, 31, 249
Böttcher M., Liang E. P., 1999, ApJ, 511, L37
Brandenburg A., Nordlund A., Stein R. F., Torkelsson U., 1995, ApJ, 446, 741
Campana S., Stella L., 1995, MNRAS, 272, 585
Churazov E., Gilfanov M., Revnivtsev M., 2001, MNRAS, 321, 759
Esin A. A., McClintock J. E., Narayan R., 1997, ApJ, 489, 865
Galeev A. A., Rosner R., Vaiana G. S., 1979, ApJ, 229, 318
George I. M., Fabian A. C., 1991, MNRAS, 249, 352
Gilfanov M., Churazov E., Revnivtsev M., 1999, A&A, 352, 182
Gilfanov M., Churazov E., Revnivtsev M., 2000, MNRAS, 316, 923
Hawley J. F., Gammie C. F., Balbus S. A., 1995, ApJ, 440, 742
Kato S., 1989, PASJ, 41, 745
Li T. P., Feng Y. X., Chen L., 1999, ApJ, 521, 789
Lynden-Bell D., Pringle J. E., 1974, MNRAS, 168, 603
Lyubarskii Y. E., 1997, MNRAS, 292, 679
Maccarone T. J., Coppi P. S., Poutanen J., 2000, ApJ, 537, L107
Magdziarz P., Zdziarski A. A., 1995, MNRAS, 273, 837
Manmoto T., Takeuchi M., Mineshige S., Matsumoto R., Negoro H., 1996, ApJ, 464, L135
Misra R., 2000, ApJ, 529, L95
Miyamoto S., Kitamoto S., Mitsuda K., Dotani T., 1988, Nat, 336, 450
Miyamoto S., Kitamoto S., 1989, Nat, 342, 773
Nayakshin S., Kallman T. R., 2001, ApJ, 546, 406
Nolan P. L. et al., 1981, ApJ, 246, 494
Nowak M. A., Wilms J., Vaughan B. A., Dove J. B., Begelman M. C., 1999b, ApJ, 515, 726
Nowak M. A., Vaughan B. A., Wilms J., Dove J. B., Begelman M. C., 1999a, ApJ, 510, 874
Pottschmidt K., Wilms J., Nowak M. A., Heindl W. A., Smith D. M., Staubert R., 2000, A&A, 357, L17
Poutanen J., 2001a, in Malaguti G., Palumbo G., eds, X-ray Astronomy 1999; Stellar Endpoints, AGN and the Diffuse Background. Gordon & Breach, Singapore, in press astro-ph/0002505)
Poutanen J., 2001b, Adv. Space Res., in press (astro-ph/0102325)
Poutanen J., Fabian A. C., 1999, MNRAS, 306, L31
Priedhorsky W., Garmire G. P., Rothschild R., Boldt E., Serlemitsos P., Holt S., 1979, ApJ, 233, 350
Revnivtsev M., Gilfanov M., Churazov E., 1999, A&A, 347, L23
Shakura N., Sunyaev R., 1973, A&A, 24, 337
Sunyaev R., Truemper J., 1979, Nat, 279, 506
van der Klis M., 1994, ApJS, 92, 511
Zdziarski A. A., Lubinski P., Smith D. A., 1999, MNRAS, 303, L11

This paper has been typeset from a TEX/LATEX file prepared by the author.